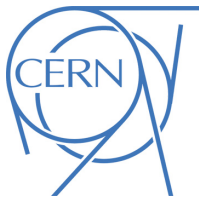




## ATLAS NOTE

ATLAS-CONF-2017-035

17th May 2017



# Search for the direct production of charginos and neutralinos in final states with tau leptons in $\sqrt{s} = 13$ TeV $pp$ collisions with the ATLAS detector

The ATLAS Collaboration

## Abstract

A search for the direct production of charginos and neutralinos in final states with at least two hadronically decaying tau leptons is presented. The analysis uses a dataset of  $pp$  collisions corresponding to an integrated luminosity of  $36.1\text{ fb}^{-1}$ , recorded with the ATLAS detector at the Large Hadron Collider at a centre-of-mass energy of  $\sqrt{s} = 13$  TeV. No significant deviation from the Standard Model background expectation is observed. Limits are derived in scenarios of  $\tilde{\chi}_1^{\pm}\tilde{\chi}_1^-$  pair production and of  $\tilde{\chi}_1^{\pm}\tilde{\chi}_2^0$  and  $\tilde{\chi}_1^+\tilde{\chi}_1^-$  production. Chargino masses up to 630 GeV are excluded at 95 % confidence level in the scenario of direct production of  $\tilde{\chi}_1^+\tilde{\chi}_1^-$  for a massless  $\tilde{\chi}_1^0$ . Common  $\tilde{\chi}_1^{\pm}, \tilde{\chi}_2^0$  masses up to 760 GeV are excluded at 95 % confidence level in the case of production of  $\tilde{\chi}_1^{\pm}\tilde{\chi}_2^0$  and  $\tilde{\chi}_1^+\tilde{\chi}_1^-$  assuming a massless  $\tilde{\chi}_1^0$ .

# 1 Introduction

Supersymmetry (SUSY) [1–7] postulates the existence of a super-partner, referred to as a *sparticle*, whose spin differs by one half unit from each corresponding Standard Model (SM) partner. In  $R$ -parity [8] conserving models, sparticles are always produced in pairs, and the lightest supersymmetric particle (LSP) is stable and provides a dark matter candidate [9–11].

In SUSY models, the sector of sparticles with only electroweak interactions contains charginos ( $\tilde{\chi}_i^\pm$ ,  $i = 1, 2$  in order of increasing masses), neutralinos ( $\tilde{\chi}_j^0$ ,  $j = 1, 2, 3, 4$  in order of increasing masses), sleptons ( $\tilde{\ell}$ ), and sneutrinos ( $\tilde{\nu}$ ). Charginos and neutralinos are the mass eigenstates formed from the linear superpositions of the super-partners of the charged and neutral Higgs bosons and electroweak gauge bosons. The sleptons are the super-partners of the leptons and are referred to as left or right ( $\tilde{\ell}_L$  or  $\tilde{\ell}_R$ ) depending on the chirality of their SM partners. The slepton mass eigenstates are a mixture of  $\tilde{\ell}_L$  and  $\tilde{\ell}_R$ , and are labelled as  $\tilde{\ell}_1$  and  $\tilde{\ell}_2$ . In this work only the  $\tilde{\chi}_1^\pm$ , the  $\tilde{\chi}_2^0$ , the  $\tilde{\chi}_1^0$ , and the scalar super-partner of the left-handed tau lepton (the stau,  $\tilde{\tau}_L$ ) and of the tau neutrino (the tau sneutrino,  $\tilde{\nu}_\tau$ ) are assumed to be sufficiently light to be produced at the Large Hadron Collider (LHC) [12].

Although experimentally challenging, final states with tau leptons are of particular interest for SUSY searches. Models with light staus can lead to a dark matter relic density consistent with cosmological observations [13], and light sleptons in general could play a role in the co-annihilation of neutralinos [14, 15]. They are expected to have masses of  $O(100$  GeV) in gauge-mediated [16–21] and anomaly-mediated [22, 23] SUSY breaking models.

Scenarios where the production of charginos, neutralinos, and sleptons may dominate at the LHC with respect to the production of squarks and gluinos can be realised in the general framework of the phenomenological Minimal Supersymmetric Standard Model (pMSSM) [24, 25]. Two simplified models [26–28] of  $\tilde{\chi}_1^+ \tilde{\chi}_1^-$  and  $\tilde{\chi}_1^\pm \tilde{\chi}_2^0$  production are considered in this work. In both models, the lightest neutralino is the LSP and purely bino, the stau and tau sneutrino are assumed to be mass-degenerate, the  $\tilde{\tau}_1$  is assumed to be purely  $\tilde{\tau}_L$ , and the mass of the  $\tilde{\tau}_L$  state is set to be halfway between those of the  $\tilde{\chi}_1^\pm$  and the  $\tilde{\chi}_1^0$ . In the model characterised by  $\tilde{\chi}_1^\pm \tilde{\chi}_2^0$  production,  $\tilde{\chi}_1^\pm$  and  $\tilde{\chi}_2^0$  are assumed to be pure wino and mass-degenerate. In the model where only  $\tilde{\chi}_1^+ \tilde{\chi}_1^-$  production is considered, the  $\tilde{\chi}_1^\pm$  is pure wino. The above assumptions guarantee large production cross sections and short decay chains for  $\tilde{\chi}_1^\pm$  and  $\tilde{\chi}_2^0$ . Charginos and next-to-lightest neutralinos decay into the lightest neutralino via an intermediate on-shell stau or tau sneutrino,  $\tilde{\chi}_1^\pm \rightarrow \tilde{\tau} \nu (\tilde{\nu}_\tau \tau) \rightarrow \tau \nu (\nu \tau) \tilde{\chi}_1^0$ ,  $\tilde{\chi}_2^0 \rightarrow \tilde{\tau} \tau \rightarrow \tau \tau \tilde{\chi}_1^0$ , and  $\tilde{\chi}_2^0 \rightarrow \tilde{\nu}_\tau \nu_\tau \rightarrow \nu_\tau \nu_\tau \tilde{\chi}_1^0$  (see Figure 1).

The direct production of chargino pairs and production of chargino and next-to-lightest neutralinos are studied using a dataset of  $\sqrt{s} = 13$  TeV  $pp$  collisions collected with the ATLAS detector in 2015 and 2016, with an integrated luminosity of  $36.1\text{ fb}^{-1}$ . Final states with at least two hadronically decaying tau leptons are considered, as this choice provides the best discrimination of SUSY events of interest from SM background processes. In a previous search from the ATLAS collaboration conducted using the 8 TeV Run-1 dataset [29],  $\tilde{\chi}_1^\pm$  masses up to 345 GeV were excluded at 95 % confidence level for a massless  $\tilde{\chi}_1^0$  in the scenario of direct production of  $\tilde{\chi}_1^+ \tilde{\chi}_1^-$ . In the case of production of  $\tilde{\chi}_1^\pm \tilde{\chi}_2^0$  and  $\tilde{\chi}_1^+ \tilde{\chi}_1^-$ , common  $\tilde{\chi}_1^\pm$ ,  $\tilde{\chi}_2^0$  masses up to 410 GeV were excluded for a massless  $\tilde{\chi}_1^0$ . Results on the Run-1 dataset from the CMS collaboration using a similar search are reported in Refs. [30, 31]. In Ref. [30], charginos lighter than 320 GeV are excluded at 95 % confidence level in the case of a massless  $\tilde{\chi}_1^0$ . The combined LEP limits on the

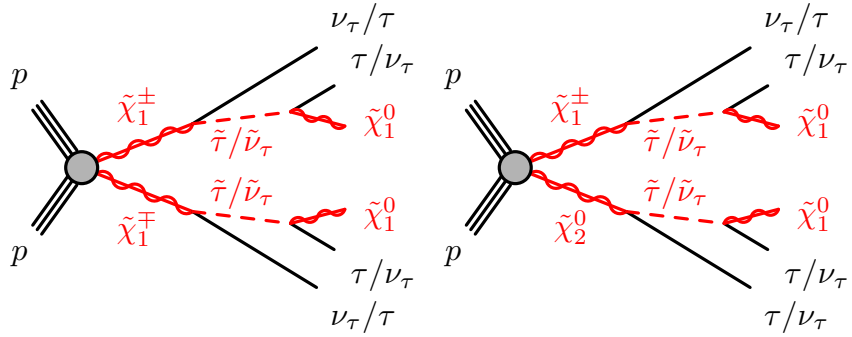


Figure 1: Representative diagrams for the electroweak production and decay processes of supersymmetric particles considered in this work: (left)  $\tilde{\chi}_1^\pm \tilde{\chi}_1^0$  and (right)  $\tilde{\chi}_1^\pm \tilde{\chi}_2^0$  production.

stau<sup>1</sup> and chargino<sup>2</sup> masses are  $m_{\tilde{\tau}} > 87\text{--}93$  GeV (depending on  $m_{\tilde{\chi}_1^0}$ ) and  $m_{\tilde{\chi}_1^\pm} > 103.5$  GeV [32–36].

## 2 The ATLAS detector

The ATLAS detector [37] is a multi-purpose particle physics detector with forward-backward symmetric cylindrical geometry and nearly  $4\pi$  coverage in solid angle<sup>3</sup>. It features an inner tracking detector (ID) surrounded by a 2 T superconducting solenoid, electromagnetic and hadronic calorimeters, and a muon spectrometer (MS). The ID covers the pseudorapidity region  $|\eta| < 2.5$  and consists of a silicon pixel detector, a silicon microstrip detector, and a transition radiation tracker. One significant upgrade for the  $\sqrt{s} = 13$  TeV running period is the presence of the Insertable B-Layer [38], an additional pixel layer close to the interaction point which provides high-resolution hits at small radius to improve the tracking and vertex reconstruction performance. The calorimeters are composed of high-granularity liquid-argon (LAr) electromagnetic calorimeters with lead, copper, or tungsten absorbers (in the pseudorapidity region  $|\eta| < 3.2$ ) and a steel–scintillator hadronic calorimeter (for  $|\eta| < 1.7$ ). The end-cap and forward regions, spanning  $1.5 < |\eta| < 4.9$ , are instrumented with LAr calorimeters for both the electromagnetic and hadronic measurements. The MS surrounds the calorimeters and consists of three large superconducting air-core toroid magnets, each with eight coils, a system of precision tracking chambers ( $|\eta| < 2.7$ ), and detectors for triggering ( $|\eta| < 2.4$ ). A two-level trigger system is used to record events [39].

## 3 Data and simulated event samples

The analysed dataset, after the application of beam, detector, and data quality requirements, corresponds to an integrated luminosity of  $36.1\text{ fb}^{-1}$  of  $pp$  collision data recorded in 2015 and 2016 at  $\sqrt{s} = 13$  TeV.

<sup>1</sup> The stau mass limit from LEP assumes gaugino mass unification, which is not assumed in the results presented here.

<sup>2</sup> For the interval  $0.1 \lesssim \Delta m(\tilde{\chi}_1^\pm, \tilde{\chi}_1^0) \lesssim 3$  GeV, the chargino mass limit set by LEP degrades to 91.9 GeV.

<sup>3</sup> ATLAS uses a right-handed coordinate system with its origin at the nominal interaction point (IP) in the centre of the detector, and the  $z$ -axis along the beam line. The  $x$ -axis points from the IP to the centre of the LHC ring, and the  $y$ -axis points upwards. Cylindrical coordinates  $(r, \phi)$  are used in the transverse plane,  $\phi$  being the azimuthal angle around the  $z$ -axis. Observables labelled *transverse* refer to the projection into the  $x$ – $y$  plane. The pseudorapidity is defined in terms of the polar angle  $\theta$  by  $\eta = -\ln \tan(\theta/2)$ .

The uncertainty in the combined 2015+2016 integrated luminosity is 3.2 %. It is derived, following a methodology similar to that detailed in Ref. [40], from a preliminary calibration of the luminosity scale using  $x - y$  beam-separation scans performed in August 2015 and May 2016. Monte Carlo (MC) simulated event samples are used to estimate the SUSY signal yields and to aid evaluating the SM backgrounds.

Events with  $Z/\gamma^* \rightarrow \ell\ell$  ( $\ell = e, \mu, \tau$ ) and  $W \rightarrow \ell\nu$  produced with accompanying jets (including light and heavy flavours) are generated at next-to-leading order (NLO) in the strong coupling constant with **SHERPA** 2.2.0 and 2.2.1 [41, 42]. Matrix elements are calculated for up to two additional partons at NLO and four additional partons at leading order (LO), using the Comix [43] and OpenLoops [44] generators and merged with the **SHERPA** parton shower (PS) [45] using the matrix element (ME)+PS@NLO prescription [42]. The NNPDF3.0NNLO [46] parton distribution function (PDF) set is used in conjunction with a dedicated parton-shower tuning developed by the **SHERPA** authors. The  $W/Z+\text{jets}$  events are normalised to their next-to-next-to-leading order (NNLO) cross sections [47]. For **SHERPA** 2.2.0 samples, a simplified scale setting prescription has been used in the multi-parton matrix elements, to improve the event generation speed.

The fully leptonic diboson processes ( $VV = WW/WZ/ZZ$ ) are generated using **SHERPA** 2.2.1 including final states with all possible combinations of charged leptons and neutrinos. The matrix elements contain all diagrams with four electroweak vertices, and they are calculated for up to one parton ( $4\ell, 2\ell+2\nu, ZZ, WW$ ) or no additional partons ( $3\ell+1\nu, 1\ell+3\nu, WZ$ ) at NLO and up to three partons at LO. The NNPDF3.0NNLO PDF set is used in conjunction with a dedicated PS tuning developed by the **SHERPA** authors. Diboson processes with one of the bosons decaying hadronically and the other leptonically are simulated using the **SHERPA** 2.1.1 generator. The matrix elements are calculated for up to one ( $ZZ$ ) or no ( $WW, WZ$ ) additional partons at NLO and up to three additional partons at LO. The CT10 [48] PDF set is used in conjunction with a dedicated PS tuning developed by the **SHERPA** authors. Each of the diboson processes is normalised to the corresponding NLO cross-section [49].

The production of top-quark pairs and single top-quarks in the  $Wt$  and  $s$ -channels is generated with **PowHEG-Box** v2 [50], with the CT10 PDF set in the ME calculations. Electroweak  $t$ -channel single top-quark events are generated using the **PowHEG-Box** v1 generator. The PS, fragmentation, and the underlying event are simulated using **PYTHIA** 6.428 [51] with the CTEQ6L1 PDF set and the corresponding Perugia 2012 tune (P2012) [52]. The **EvtGen** v1.2.0 program [53] is used for properties of the bottom and charm hadron decays. The top-quark mass is set to 172.5 GeV. The overall cross section is computed at NNLO in  $\alpha_s$ , including resummation of next-to-next-to-leading logarithmic (NNLL) soft gluon terms [54] for  $t\bar{t}$ , to NLO+NNLL accuracy for single top-quark  $Wt$ -channel [55], and to NLO for the  $t$ - and  $s$ -channels [56]. Top-quark pair production with an additional  $W$  or  $Z$  boson is generated using **MADGRAPH5\_aMC@NLO** v2.2.2 [57], while fragmentation and hadronisation are simulated with **PYTHIA** 8.186 [58]. The ATLAS underlying-event tune A14 [59] is used with the NNPDF2.3LO [60] PDF set, the cross sections are normalised to NLO [61, 62].

Simulated signal samples are generated using **MADGRAPH5\_aMC@NLO** v2.2.3 interfaced to **PYTHIA** 8.186 with the A14 tune for the PS modelling, hadronisation, and underlying event. The ME calculation is performed at tree-level and includes the emission of up to two additional partons. The PDF set used for the generation is NNPDF2.3LO. The ME-PS matching is done using the CKKW-L [63] prescription, with a matching scale set to one quarter of the mass of the pair of produced particles. Signal cross sections are calculated to next-to-leading order in the strong coupling constant, adding the resummation of soft gluon emission at next-to-leading-logarithmic accuracy (NLO+NLL) [64, 65]. The nominal cross section and the uncertainty are taken from an envelope of cross-section predictions using different PDF sets and factorisation and renormalisation scales, as described in Ref. [66].

Two simplified models characterised by  $\tilde{\chi}_1^+ \tilde{\chi}_1^-$  and  $\tilde{\chi}_1^\pm \tilde{\chi}_2^0$  production are considered. In these models, all sparticles other than  $\tilde{\chi}_1^\pm$ ,  $\tilde{\chi}_2^0$ ,  $\tilde{\chi}_1^0$ ,  $\tilde{\tau}_L$  and  $\tilde{\nu}_\tau$  are assumed to be not accessible at the LHC energy. The neutralinos and charginos decay via intermediate staus and tau sneutrinos. In both models, the  $\tilde{\chi}_1^\pm$  mass is varied between 100 GeV and 1.1 TeV, and the  $\tilde{\chi}_1^0$  mass is varied between zero and 500 GeV. The cross section for  $\tilde{\chi}_1^\pm \tilde{\chi}_2^0$  ( $\tilde{\chi}_1^+ \tilde{\chi}_1^-$ ) production ranges from 23 (11.6) pb for a  $\tilde{\chi}_1^\pm$  mass of 100 GeV to 0.74 (0.343) fb for a  $\tilde{\chi}_1^\pm$  mass of 1.1 TeV.

Two reference points are used throughout this paper to illustrate the typical features of the SUSY models to which this analysis is sensitive:

- Reference point 1: simplified model for  $\tilde{\chi}_1^\pm \tilde{\chi}_2^0$  production with the masses of the  $\tilde{\chi}_1^\pm$  and the  $\tilde{\chi}_2^0$  equal to 600 GeV, and a massless  $\tilde{\chi}_1^0$ ;
- Reference point 2: simplified model for  $\tilde{\chi}_1^+ \tilde{\chi}_1^-$  production with the mass of the  $\tilde{\chi}_1^\pm$  equal to 600 GeV, and a massless  $\tilde{\chi}_1^0$ .

SM samples are processed through a detailed detector simulation [67] based on GEANT 4 [68], whereas SUSY samples are passed through a fast detector simulation based on a parametrisation of the performance of the ATLAS electromagnetic and hadronic calorimeters [69]. The simulated events are reconstructed using the same algorithms as the data, and are reweighted so that the distribution of the expected number of collisions per bunch crossing matches the one in the data. All simulated events are overlaid with multiple  $pp$  collisions (pile-up) simulated with the soft strong interaction processes of PYTHIA 8.186 using the A2 set of tunable parameters [70] and the MSTW2008LO [71] PDF set.

## 4 Event and object reconstruction

Events with at least one reconstructed primary vertex [72] are selected. A primary vertex must have at least two associated charged-particle tracks with transverse momentum  $p_T > 400$  MeV and be consistent with the beam spot envelope. If there are multiple primary vertices in an event, the one with the largest  $\sum p_T^2$  of the associated tracks is chosen.

Jets are reconstructed from three-dimensional calorimeter energy clusters [73] using the anti- $k_t$  algorithm [74, 75] with a radius parameter of 0.4. Jet energies are corrected for detector inhomogeneities, the non-compensating response of the calorimeter, and the impact of pile-up, using factors derived from test beam and  $pp$  collision data, and from a detailed GEANT 4 detector simulation [76, 77]. The impact of pile-up is accounted for using a technique, based on jet areas, that provides an event-by-event and jet-by-jet correction [78]. Jets that are likely to have originated from pile-up are not considered [79]. Jets are required to have  $p_T > 20$  GeV and  $|\eta| < 2.8$ . Events containing jets that are likely to have arisen from detector noise or cosmic rays are removed.

Jets containing  $b$ -hadrons ( $b$ -jets) are identified using the MV2c10 algorithm, a multivariate discriminant making use of track impact parameters and reconstructed secondary vertices [80]. Candidate  $b$ -jets are required to have  $p_T > 20$  GeV and  $|\eta| < 2.5$ . A working point with an average  $b$ -tagging efficiency of 77 % for simulated  $t\bar{t}$  events is used [81, 82]. The rejection factors for light-quark and gluon jets,  $c$ -quark jets, and hadronically decaying tau leptons are approximately 134, 6, and 55, respectively.

Electron candidates are reconstructed by matching clusters in the electromagnetic calorimeter with charged particle tracks in the inner detector. Electrons are required to have  $p_T > 10$  GeV,  $|\eta| < 2.47$ , and to satisfy

the ‘loose’ working point according to a likelihood-based identification [83]. Muon candidates are identified by matching an extrapolated inner detector track and one or more track segments in the muon spectrometer. Muons are required to have  $p_T > 10$  GeV and  $|\eta| < 2.7$  and fulfil the ‘medium’ quality criteria of Ref. [84]. Events containing a muon candidate with a poorly measured charge-to-momentum ratio ( $\sigma(q/p) / |q/p| > 0.2$ ) are rejected. Events are required not to contain any candidate muon with high impact parameters ( $|z_0| > 1$  mm or  $|d_0| > 0.2$  mm), as these may originate from cosmic rays. The efficiencies for electrons and muons to satisfy the reconstruction, identification, and isolation criteria are measured in samples of  $Z$  and  $J/\psi$  leptonic decays, and corrections are applied to the simulated samples to reproduce the efficiencies in data.

The reconstruction of hadronically decaying tau leptons is based on the information from tracking in the ID and three-dimensional clusters in the electromagnetic and hadronic calorimeters. The tau reconstruction algorithm is seeded by jets reconstructed as described above but with  $p_T > 10$  GeV and  $|\eta| < 2.5$ . The reconstructed energies of the hadronically decaying tau candidates are corrected to the tau energy scale, which is calibrated using tau-energy-scale corrections based on simulation and in-situ measurements using  $Z \rightarrow \tau\tau$  decays. Tau neutrinos from the tau lepton decay are not taken into account in the reconstruction and calibration of the tau energy and momentum. Since hadronic tau leptons decay mostly to either one or three charged pions, together with a neutrino and often additional neutral pions, tau candidates are required to have one or three associated charged particle tracks (prongs) and the total electric charge of those tracks must be  $\pm 1$  times the electron charge. To improve the discrimination between hadronically decaying tau leptons and jets, electrons, or muons, multivariate algorithms are used [85]. The tau identification algorithm is based on a Boosted Decision Tree (BDT) method. The BDT algorithms use various track and cluster variables as input to discriminate tau leptons from jets. For 1-prong (3-prong) tau candidates, the signal efficiencies are 60 % (50 %), 55 % (40 %), and 45 % (30 %) for the ‘loose’, ‘medium’, and ‘tight’ working points, respectively. In the following, tau candidates are required to pass the medium identification criteria for jet discrimination (‘medium’ tau candidates), unless otherwise stated. For electron discrimination, an overlap-based veto is used. This requirement has about 95 % efficiency, and a rejection factor from 10 to 50 depending on the  $\eta$  range. Tau candidates are required to have  $p_T > 20$  GeV and  $|\eta| < 2.47$ , excluding the transition region between the barrel and end-cap calorimeters ( $1.37 < |\eta| < 1.52$ ).

The simulation is corrected for differences in the efficiency of the tau identification and trigger algorithms between data and simulation. For hadronically decaying tau leptons originating from prompt gauge boson decays, the corrections are calculated with a *tag-and-probe* method in a sample of  $Z \rightarrow \tau\tau$  events where one tau lepton decays hadronically and the other leptonically into a muon and two neutrinos [86].

The measurement of the missing transverse momentum vector,  $\mathbf{p}_T^{\text{miss}}$ , and its magnitude,  $E_T^{\text{miss}}$ , is based on the negative vectorial sum of the  $\mathbf{p}_T$  of reconstructed objects (jets, tau candidates, electrons, photons, muons) and an additional soft term. The soft term is constructed from all high-quality tracks that are not associated with any physics object, and that are associated to the primary vertex. In this way, the missing transverse momentum is adjusted for the best calibration of the jets and the other identified physics objects, while maintaining pile-up independence in the soft term [87, 88].

The possible double counting of reconstructed objects is resolved in the following order. Tau candidates close to electron or muon candidates ( $\Delta R < 0.2$ , where  $\Delta R = \sqrt{(\Delta y)^2 + (\Delta\phi)^2}$ ) are removed, as are electrons that share a track with a muon. For electrons close to a jet ( $\Delta R < 0.4$ ), the electron is removed, except when  $\Delta R < 0.2$  and the jet is not  $b$ -tagged, in which case the jet is removed. Any remaining jet within  $\Delta R < 0.4$  of a muon or tau candidate is removed.

## 5 Event selection

The events used in this analysis are recorded using either an *asymmetric di-tau* trigger or a combined *di-tau +  $E_T^{\text{miss}}$*  trigger. The asymmetric di-tau trigger requires the identification of two hadronically decaying tau candidates with  $p_{\text{T},\tau_1} > 85$  GeV and  $p_{\text{T},\tau_2} > 50$  GeV GeV at trigger-level for the leading and next-to-leading tau candidates respectively. Two tau candidates with  $p_{\text{T},\tau_1} > 35$  GeV and  $p_{\text{T},\tau_2} > 25$  GeV GeV at trigger-level, and  $E_T^{\text{miss}} > 50$  GeV (at uncalibrated electromagnetic scale) are required by the di-tau +  $E_T^{\text{miss}}$  trigger. In events selected by the di-tau +  $E_T^{\text{miss}}$  trigger, the reconstructed  $E_T^{\text{miss}}$  must be larger than 150 GeV. The trigger efficiency for correctly identified tau leptons is  $\sim 80\%$  for events where the leading tau candidate has  $p_{\text{T}} > 95$  (50) GeV at reconstruction level, the next-to-leading tau candidate has  $p_{\text{T}} > 65$  (40) GeV for the asymmetric ditau (di-tau +  $E_T^{\text{miss}}$ ) trigger. In events selected by the di-tau +  $E_T^{\text{miss}}$  trigger, the reconstructed  $E_T^{\text{miss}}$  must be larger than 150 GeV.

Events are required to have at least two tau candidates with opposite electrical charge. The invariant mass of any opposite-sign (OS) tau pair must be larger than 12 GeV to remove tau leptons originating from low-mass resonances. This requirement has negligible effect on the signal efficiency. Two of the reconstructed tau candidates must satisfy the  $p_{\text{T}}$  requirements to be in the region where the trigger efficiency is constant.

To further discriminate the SUSY signal events from SM background processes, additional requirements are applied to define the so-called signal region (SR) selections. To reject events from SM processes containing a top quark, selected events must not contain any  $b$ -tagged jet (*b-jet veto*). To suppress SM backgrounds with a  $Z$  boson, events are selected by requiring that the reconstructed invariant mass of all oppositely charged tau pairs,  $m(\tau_1, \tau_2)$ , must not be within 10 GeV of the mean visible  $Z$  boson mass<sup>4</sup> (79 GeV). This requirement is referred to as the *Z-veto*.

The *transverse* mass  $m_{\text{T}2}$  [89, 90] is defined as:

$$m_{\text{T}2} = \min_{\mathbf{q}_{\text{T}}} \left[ \max \left( m_{\text{T},\tau_1}(\mathbf{p}_{\text{T},\tau_1}, \mathbf{q}_{\text{T}}), m_{\text{T},\tau_2}(\mathbf{p}_{\text{T},\tau_2}, \mathbf{p}_{\text{T}}^{\text{miss}} - \mathbf{q}_{\text{T}}) \right) \right],$$

where  $\mathbf{p}_{\text{T},\tau_1}$  and  $\mathbf{p}_{\text{T},\tau_2}$  are the transverse momenta of the two tau candidates, and  $\mathbf{q}_{\text{T}}$  is the transverse vector that minimises the larger of the two transverse masses  $m_{\text{T},\tau_1}$  and  $m_{\text{T},\tau_2}$ . The latter masses are defined by

$$m_{\text{T}}(\mathbf{p}_{\text{T}}, \mathbf{q}_{\text{T}}) = \sqrt{2(p_{\text{T}}q_{\text{T}} - \mathbf{p}_{\text{T}} \cdot \mathbf{q}_{\text{T}})}.$$

In events where more than two tau candidates are selected,  $m_{\text{T}2}$  is computed among all possible tau pairs and the combination leading to the largest value is chosen. For  $t\bar{t}$  and  $WW$  events, in which two  $W$  bosons decay leptonically and  $\mathbf{p}_{\text{T}}^{\text{miss}}$  is the sum of the transverse momenta of the two neutrinos, the  $m_{\text{T}2}$  distribution has a kinematic end-point at the  $W$  mass. For large mass differences between the next-to-lightest neutralinos, the charginos, or the staus and the lightest neutralino, the  $m_{\text{T}2}$  distribution for signal events extends significantly beyond this end-point.

Two SRs based on large  $m_{\text{T}2}$  and  $E_T^{\text{miss}}$  requirements are defined. SR-lowMass (SR-highMass) is designed to cover signal models where the mass difference between the  $\tilde{\chi}_1^{\pm}$  and  $\tilde{\chi}_1^0$  is smaller (larger) than 200 GeV. In SR-lowMass, only the di-tau+ $E_T^{\text{miss}}$  trigger is used. This trigger has high efficiency in selecting events

<sup>4</sup> The mean visible  $Z$  boson mass is defined as the mean value of a Gaussian fit of the reconstructed invariant mass distribution of OS tau pairs in a MC sample of  $Z \rightarrow \tau\tau$  events with associated jets.

with tau leptons originating from  $\tilde{\chi}_1^\pm$  and  $\tilde{\chi}_2^0$  decays in models where the mass difference between the parent particle and the  $\tilde{\chi}_1^0$  is small. The main discriminating requirement is  $m_{T2} > 70$  GeV.

In SR-highMass events are selected with the di-tau+ $E_T^{\text{miss}}$  trigger or by the asymmetric di-tau trigger. In the case the event has been selected by the di-tau+ $E_T^{\text{miss}}$  trigger, the leading tau candidate threshold is raised to  $p_{T,\tau_1} > 80$  GeV. If the event has been selected by the asymmetric di-tau trigger,  $E_T^{\text{miss}} > 110$  GeV is required. At least one of the tau candidates must satisfy the tight identification criteria for jet discrimination ('tight' tau candidate). In addition, the invariant mass of the two leading tau candidates,  $m(\tau_1, \tau_2) > 110$  GeV, and  $m_{T2} > 90$  GeV. The requirements for both SRs are summarised in Table 1. The two SRs are not mutually exclusive.

Table 1: Signal region definitions.

SR-lowMass	SR-highMass
at least one opposite sign tau pair $b$ -jet veto $Z$ -veto	$m(\tau_1, \tau_2) > 110$ GeV $m_{T2} > 90$ GeV at least one medium and one tight tau candidates $m(\tau_1, \tau_2) > 110$ GeV $m_{T2} > 90$ GeV di-tau+ $E_T^{\text{miss}}$ trigger $E_T^{\text{miss}} > 150$ GeV $p_{T,\tau_1} > 50$ GeV $p_{T,\tau_2} > 40$ GeV
at least two medium tau candidates $m_{T2} > 70$ GeV di-tau+ $E_T^{\text{miss}}$ trigger $E_T^{\text{miss}} > 150$ GeV $p_{T,\tau_1} > 50$ GeV $p_{T,\tau_2} > 40$ GeV	di-tau+ $E_T^{\text{miss}}$ trigger $E_T^{\text{miss}} > 150$ GeV $p_{T,\tau_1} > 80$ GeV $p_{T,\tau_2} > 40$ GeV asymmetric di-tau trigger $E_T^{\text{miss}} > 110$ GeV $p_{T,\tau_1} > 95$ GeV $p_{T,\tau_2} > 65$ GeV

## 6 Standard Model background estimation

The main SM processes contributing to the selected final states are multi-jet,  $W$ +jets and diboson production. Background events may contain a combination of 'real' tau leptons, defined as correctly identified tau leptons, or 'fake' tau leptons, which can originate from a misidentified light-flavour quark or gluon jet, an electron, or a muon.

In multi-jet events nearly all tau candidates are misidentified jets. The multi-jet contribution in the SRs is estimated from data, as described in Section 6.1. The contribution arising from heavy-flavour multi-jet events containing a real tau lepton from the heavy-flavour quark decay is included in the multi-jet estimate. The contribution of  $W$ +jets events, which contain one real tau lepton from the  $W$  decay and one or more misidentified jets, is estimated from MC simulation and normalised to data in a dedicated control region (CR), as described in Section 6.2.

Diboson production contributes mainly with events containing real tau leptons originating from  $WW$  and  $ZZ$  decaying into a  $\tau\tau\nu\nu$  final state. Additional SM backgrounds arise from  $Z$ +jets production, or events that contain a top-quark or a top-quark pair in association with jets or additional  $W$  or  $Z$  bosons (collectively referred to as *top* background in the following). The contribution from real tau leptons exceeds 90 % in  $Z$ +jets and diboson production, and ranges from 45 % to 75 % in backgrounds containing top quarks from MC simulation. The contribution of fake tau leptons from heavy-flavour decays in jets is

negligible. To estimate the irreducible background, which includes diboson,  $Z$ +jets and top-quark events, only MC simulated samples are used, as described in Section 6.3.

The sources of systematic uncertainty on the background estimates are described in Section 7. For each signal region a simultaneous fit based on the profile likelihood method [91] is performed to normalise the multi-jet and  $W$ +jets background estimates, as described in Section 8.

## 6.1 Multi-jet background estimation

One of the dominant backgrounds in the SRs originates from jets misidentified as tau leptons in multi-jet production. This contribution is estimated from data using the so-called *ABCD* method. Four exclusive regions, labelled as A, B, C, and D, are defined in a two-dimensional plane as a function of two (or more) uncorrelated discriminating variables. The ratio of events in the regions C and B equals to that in the regions D and A. The number of events in region D,  $N_D$ , can therefore be calculated from that in region A,  $N_A$ , multiplied by the transfer factor  $T = N_C/N_B$ . In this case, the region D corresponds to one of the SRs defined in Section 5 (SR-lowMass or SR-highMass), whereas the regions A, B, and C are control regions defined accordingly. In the following the regions A, B, C, D are labelled as CR-A, CR-B, CR-C, and SR-D.

The tau identification criteria (loose, medium or tight as defined in Section 4), the electric charge of the tau pair (OS or same sign, SS),  $m(\tau_1, \tau_2)$ ,  $\Delta R(\tau_1, \tau_2)$ ,  $m_{T2}$ , and  $E_T^{\text{miss}}$  are used to define CR-A, CR-B, and CR-C. Furthermore, two sets of validation regions (VR), VR-E and VR-F, are defined corresponding to each SR. The validation regions are used to verify the extrapolation of the ABCD estimation to the SRs and to estimate the systematic uncertainty from the residual correlation between the tau identification and charge requirements, and the kinematic variables  $m_{T2}$  and  $E_T^{\text{miss}}$ . All regions used for the ABCD method are schematically drawn in Figure 2, and defined in Table 2.

In all validation regions and both sets of CR-B and CR-C, events are recorded using a *di-tau* trigger instead of the *di-tau* +  $E_T^{\text{miss}}$  trigger, due to the low  $E_T^{\text{miss}}$  requirements. The *di-tau* trigger requires the identification of two hadronically decaying tau candidates with transverse momenta exceeding a set of thresholds, similar to those described in Section 5. The *di-tau* trigger was pre-scaled during all 2016 data taking.

The number of multi-jet events in the control and validation regions is estimated from data after subtraction of other SM contributions estimated from MC simulation. In both CR-B and VR-E more than 86 % of the events come from multi-jet production, whereas for CR-A and CR-C the multi-jet purity is larger than 47 % and 68 %, respectively. Good agreement between data and SM backgrounds is found for the  $E_T^{\text{miss}}$  and  $m_{T2}$  distributions in the validation regions, as shown in Figure 3. The results of the ABCD method for the multijet event yields in the signal regions are summarised in Table 7.

The signal contamination in a certain region is defined as the ratio of the number of signal events and the sum of the number of signal events and SM background processes. The signal contamination in CR-A for both SRs ranges from a few percent to 30–50 % for a few signal models, and it is taken into account in the simultaneous fit described in Section 8. The largest contaminations are found for a  $\tilde{\chi}_1^\pm$  mass of 400 GeV and massless  $\tilde{\chi}_1^0$  for  $\tilde{\chi}_1^+ \tilde{\chi}_1^-$  production, and for a  $\tilde{\chi}_1^\pm$  mass of 300 GeV and massless  $\tilde{\chi}_1^0$  for  $\tilde{\chi}_1^\pm \tilde{\chi}_2^0$  production. The possible presence of a non-SM signal in CR-A has been tested and proved not to change the fit results significantly.

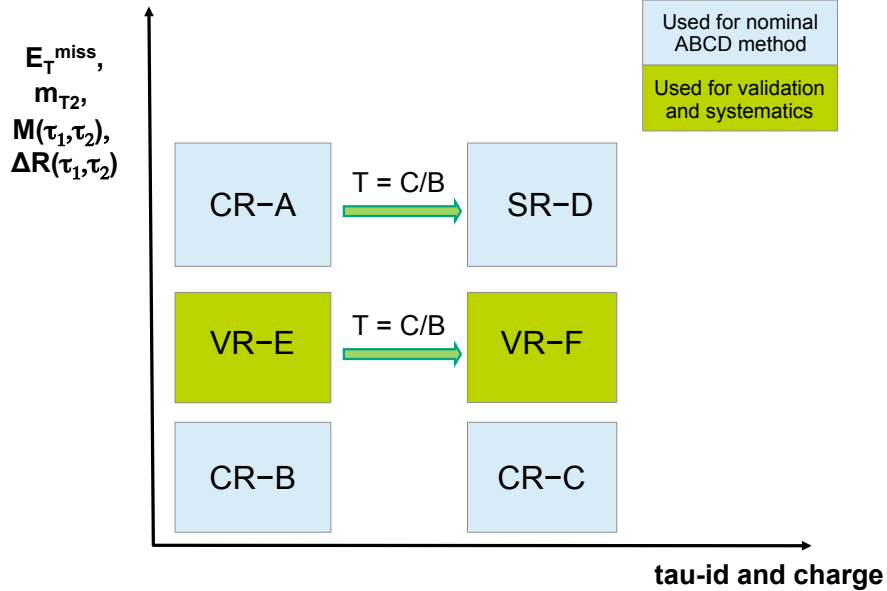


Figure 2: Illustration of the ABCD method for the multi-jet background determination. The control regions A, B, C, and signal region D for the ABCD method described in the text (labelled as CR-A, CR-B, CR-C and SR-D) are drawn as light blue boxes. Shown in green and labelled as VR are the regions E and F, which are used to validate the ABCD method and to estimate the systematic uncertainties. The definition of all regions used in the ABCD method can be found in Table 2.

## 6.2 $W$ +jets background estimation

The production of  $W$ +jets events with at least one misidentified tau lepton is an important background in the SRs, making up for about 13 % (20 %) of the expected SM background in SR-lowMass (SR-highMass). A dedicated control region ( $W$ -CR) is used to normalise the  $W$ +jets MC estimation to data. The  $W$ -CR is enriched in events where the  $W$  boson decays leptonically into a muon and a neutrino to suppress multi-jet contamination. Events are selected with a single-muon trigger, using the lowest unprescaled  $p_T$  thresholds available. Events containing exactly one isolated muon and one candidate tau lepton with opposite electric charge are selected. The muon is required to have  $p_T > 40$  GeV. In addition, the muon must satisfy the ‘GradientLoose’ [92] isolation requirements, which rely on the use of track-based and calorimeter-based variables and implement a set of  $\eta$ - and  $p_T$ -dependent criteria. Compatibility of the signal lepton tracks with the primary vertex is enforced by requiring the distance  $|z_0 \sin \theta| < 0.5$  mm, where  $z_0$  is the longitudinal impact parameter. In addition, the transverse impact parameter,  $d_0$ , divided by its uncertainty,  $\sigma(d_0)$ , must satisfy  $|d_0/\sigma(d_0)| < 3$  for the muon. The tau candidate must pass the medium tau identification criteria and is required to have  $p_T > 50$  GeV.

The contribution from events with top quarks is suppressed by rejecting events containing  $b$ -tagged jets. To reduce the contribution from  $Z$ +jets production, the transverse mass of the muon,  $m_{T,\mu} > 50$  GeV, the sum of the transverse mass of the tau lepton and muon,  $m_{T,\tau} + m_{T,\mu} > 80$  GeV, and the angular separation between the muon and the tau lepton,  $\Delta R(\mu, \tau) > 0.5$  are required. To further suppress diboson and top quark contributions,  $m_{\tau,\mu} < 150$  GeV is required. To be close to the SR definition,  $E_T^{\text{miss}} > 60$  GeV and

Table 2: Definition of the regions used in the ABCD method for the multi-jet estimation in SR-lowMass (left) and SR-highMass (right). Only those requirements that are different in the CRs/VRs with respect to the SRs are listed.

CR-A	SR-D (SR-lowMass)	CR-A	SR-D (SR-highMass)
di-tau+ $E_T^{\text{miss}}$ trigger		di-tau+ $E_T^{\text{miss}}$ or asymmetric di-tau trigger	
$\geq 2$ loose tau leptons (SS)	$\geq 2$ medium tau leptons (OS)	$\geq 2$ loose tau leptons (OS)	$\geq 2$ medium tau leptons (OS)
$m(\tau_1, \tau_2) < 250$ GeV		$< 1$ medium 1 tight tau leptons	$\geq 1$ tight tau lepton
$\Delta R(\tau_1, \tau_2) > 1.5$		$\Delta R(\tau_1, \tau_2) > 1.8$	
$E_T^{\text{miss}} > 150$ GeV	$E_T^{\text{miss}} > 150$ GeV	$E_T^{\text{miss}} > 110$ GeV	
$m_{T2} > 70$ GeV	$m_{T2} > 70$ GeV	$m_{T2} > 90$ GeV	$m_{T2} > 90$ GeV
VR-E		VR-F	
di-tau trigger		di-tau or asymmetric di-tau trigger	
$\geq 2$ loose tau leptons (SS)	$\geq 2$ medium tau leptons (OS)	$\geq 2$ loose tau leptons (OS)	$\geq 2$ medium tau leptons (OS)
$m(\tau_1, \tau_2) < 250$ GeV		$< 1$ medium 1 tight tau leptons	$\geq 1$ tight tau lepton
$\Delta R(\tau_1, \tau_2) > 1.5$		$\Delta R(\tau_1, \tau_2) > 1.8$	
$E_T^{\text{miss}} > 40$ GeV	$E_T^{\text{miss}} > 40$ GeV	$E_T^{\text{miss}} > 40$ GeV	
$50 < m_{T2} < 70$ GeV	$50 < m_{T2} < 70$ GeV	$60 < m_{T2} < 90$ GeV	$60 < m_{T2} < 90$ GeV
CR-B		CR-C	
di-tau trigger		di-tau or asymmetric di-tau trigger	
$\geq 2$ loose tau leptons (SS)	$\geq 2$ medium tau leptons (OS)	$\geq 2$ loose tau leptons (OS)	$\geq 2$ medium tau leptons (OS)
$m(\tau_1, \tau_2) < 250$ GeV		$< 1$ medium 1 tight tau leptons	$\geq 1$ tight tau
$\Delta R(\tau_1, \tau_2) > 1.5$		$\Delta R(\tau_1, \tau_2) > 1.8$	
$E_T^{\text{miss}} > 40$ GeV	$E_T^{\text{miss}} > 40$ GeV	$E_T^{\text{miss}} > 40$ GeV	
$20 < m_{T2} < 50$ GeV	$20 < m_{T2} < 50$ GeV	$10 < m_{T2} < 60$ GeV	$10 < m_{T2} < 60$ GeV

the invariant mass of the muon and tau lepton,  $m(\mu, \tau) > 70$  GeV are required. Events in the  $W$ -CR are selected by requiring low  $m_{T2}$ , while a high  $m_{T2}$  region is used to validate the  $W$ +jets estimate ( $W$  validation region,  $W$ -VR). The definitions of the  $W$ -CR and  $W$ -VR are given in Table 3.

The multi-jet contribution in the  $W$ -CR (-VR) is estimated using the so-called *OS-SS* method by counting the number of events in data satisfying the same requirements as the  $W$ -CR (-VR) but with the charge of the two leptons having the same-sign (SS). Events from SM processes other than multi-jet production are subtracted from the data counts in the SS region using their MC prediction. The *OS-SS* method relies on the fact that in the multi-jet background the ratio of SS to OS events is close to unity, while a significant difference from unity is expected for  $W$ +jets production. The latter is dominated by  $gu/gd$ -initiated processes that often give rise to a jet originating from a quark, the charge of which is anti-correlated with the  $W$ -boson charge. Based on studies with simulated samples, a systematic uncertainty of 100 % is assigned to the multi-jet estimation in the  $W$ -CR.

The event yields in the  $W$ -CR and  $W$ -VR are given in Table 4. The purity of the selection in  $W$ +jets events is around 72 % (77 %) in the  $W$ -CR (VR). Good agreement between data and SM predictions is observed. The signal contamination in the  $W$ -CR and  $W$ -VR is negligible. Distributions of the kinematic variables defining the SRs are shown in Figure 4, in which the contribution of  $W$ +jets events is scaled with the normalisation factor 1.02 obtained from the fit described in Section 8.

### 6.3 Irreducible background estimation

Irreducible SM backgrounds arise mainly from  $t\bar{t}$ , single top quark,  $t\bar{t}+V$ ,  $Z/\gamma^*+{\text{jets}}$ , and diboson ( $WW$ ,  $WZ$  and  $ZZ$ ) processes and are estimated with MC simulation. Other SM backgrounds are negligible.

The inclusive contribution from  $t\bar{t}$ , single top quark,  $t\bar{t}+V$  and  $Z/\gamma^*+{\text{jets}}$  amounts to about 18 % (13 %) of the total background in the SR-highMass (SR-lowMass). The MC estimates are validated in regions

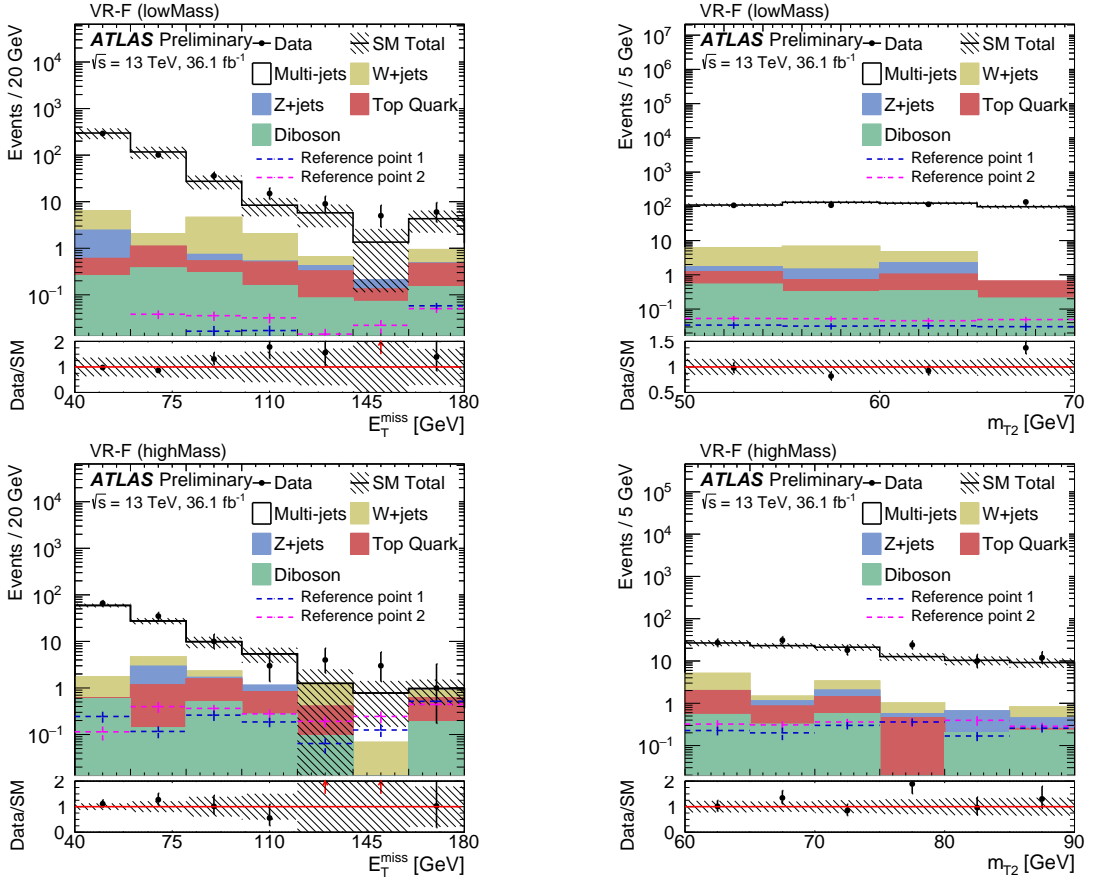


Figure 3: The  $E_T^{\text{miss}}$  (left) and  $m_{T2}$  (right) distributions in the multi-jet background VR-F for SR-lowMass (top) and VR-F for SR-highMass (bottom). The stacked histograms show the contribution of the non-multi-jet SM backgrounds from MC simulation, normalised to  $36.1 \text{ fb}^{-1}$ . The multi-jet contribution is estimated from data using the ABCD method. The hatched bands represent the combined statistical and systematic uncertainties on the sum of the SM backgrounds shown. For illustration, the distributions of the SUSY reference points (defined in Section 3) are also shown as dashed lines. The last bin includes the overflow.

Table 3: The W-CR (left) and W-VR (right) definitions.

W-CR	W-VR
one isolated muon and one medium tau lepton with opposite sign $b$ -jet veto $m(\mu, \tau) > 70 \text{ GeV}$ $E_T^{\text{miss}} > 60 \text{ GeV}$ $50 \text{ GeV} < m_{T,\mu} < 150 \text{ GeV}$ $m_{T,\mu} + m_{T,\tau} > 80 \text{ GeV}$ $0.5 < \Delta R(\mu, \tau) < 3.5$ $10 \text{ GeV} < m_{T2} < 60 \text{ GeV}$	

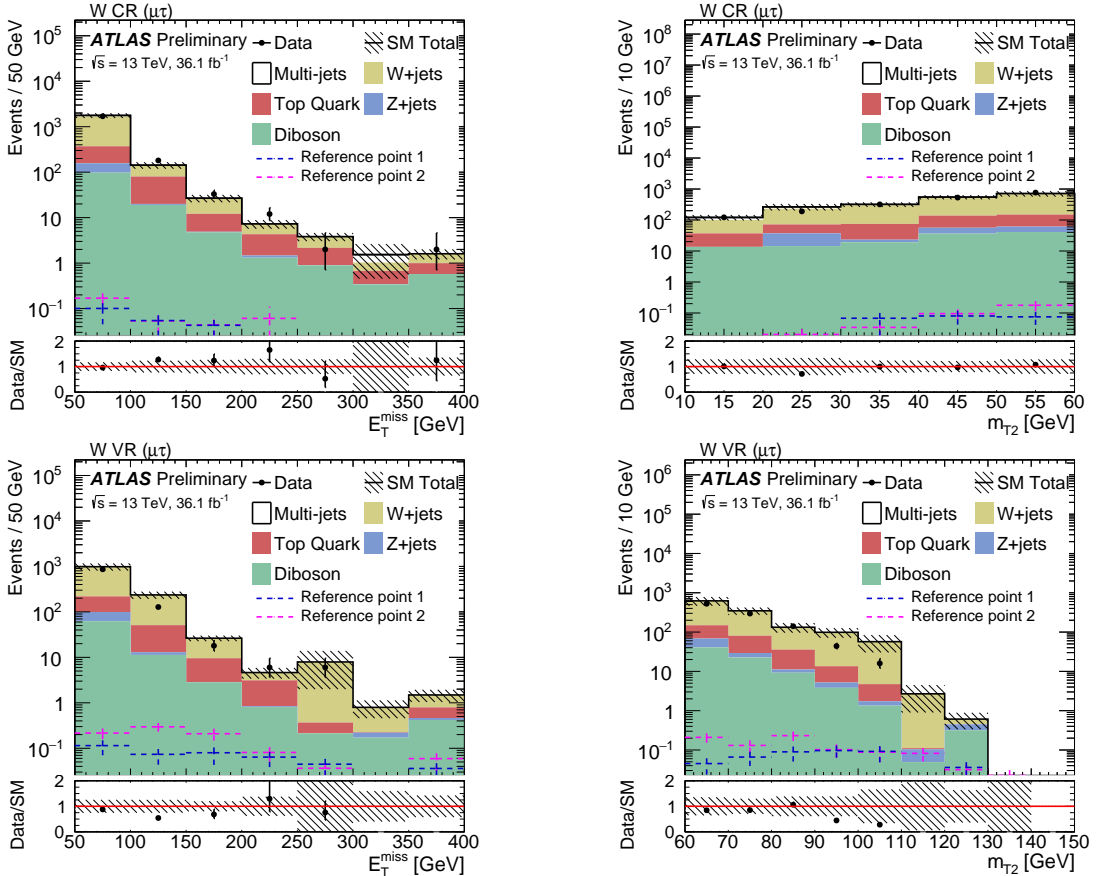


Figure 4: The  $E_T^{\text{miss}}$  (left) and  $m_{T2}$  (right) distributions in the  $W$ -CR (top) and  $W$ -VR (bottom). The SM backgrounds other than multi-jet production are estimated from MC simulation and normalised to  $36.1 \text{ fb}^{-1}$ . The contribution of  $W$ -jets events is scaled with the normalisation factor 1.02 obtained from the fit described in Section 8. The multi-jet contribution is estimated from data using the  $OS$ - $SS$  method. The hatched bands represent the combined statistical and systematic uncertainties on the total SM background. For illustration, the distributions of the SUSY reference points (defined in Section 3) are also shown as dashed lines. The lower panels show the ratio of data to the SM background estimate. The last bin includes the overflow.

Table 4: Event yields in the  $W$ -CR and  $W$ -VR. The SM backgrounds other than multi-jet production are estimated from MC simulation and normalised to  $36.1 \text{ fb}^{-1}$ . The contribution of  $W$ +jets events is scaled with the normalisation factor obtained from the fit described in Section 8. The multi-jet contribution is estimated from data using the OS-SS method. In the  $W$ -VR the multi-jet estimation with the OS-SS method yields a negative contribution, which is set to zero. The shown uncertainties are the sum in quadrature of statistical and systematic uncertainties. The correlation of systematic uncertainties among control and validation regions and background processes is fully taken into account in the fit.

Sample	$W$ -CR	$W$ -VR
Data	1928	1023
SM total	$1930 \pm 50$	$1260 \pm 440$
$W$ +jets	$1395 \pm 130$	$980 \pm 410$
$Z$ +jets	$60 \pm 28$	$39 \pm 15$
Diboson	$125 \pm 24$	$78 \pm 20$
Top quark	$290 \pm 80$	$170 \pm 60$
Multi-jet	$60 \pm 60$	$0 \pm 100$
Reference point 1	$0.22 \pm 0.07$	$0.44 \pm 0.08$
Reference point 2	$0.33 \pm 0.08$	$0.87 \pm 0.11$

enriched in  $Z/\gamma^*$ +jets and top-quark events. For both regions, events are recorded using either a combined di-tau +  $E_T^{\text{miss}}$  trigger or an asymmetric di-tau trigger. Events are required to have at least two tau candidates with opposite electric charge,  $E_T^{\text{miss}} > 150 \text{ GeV}$ , and leading (sub-leading) tau  $p_T > 50$  (40)  $\text{GeV}$ . In the  $Z/\gamma^*$ +jets validation region ( $Z$ -VR) at least two tau candidates must satisfy the medium tau identification criteria. To suppress top-quark backgrounds, events containing  $b$ -jets are vetoed. To further enhance the purity of  $Z/\gamma^*$ +jets events,  $m_{T2} < 10 \text{ GeV}$  has been required. In the top-quark validation region (Top-VR) at least one tau candidate must satisfy the medium tau identification criteria. To increase the contribution from top-quark events, events must contain at least one  $b$ -tagged jet with  $p_T > 20 \text{ GeV}$  and should be kinematically compatible with  $t\bar{t}$  production (top-tagged) through the use of the *contransverse* mass  $m_{\text{CT}}$  [93]. The scalar sum of the  $p_T$  of the two tau leptons and of at least one combination of two jets in an event must exceed  $100 \text{ GeV}$ . Top-tagged events are required to possess  $m_{\text{CT}}$  values calculated from combinations of jets and tau leptons consistent with the expected bounds from  $t\bar{t}$  events as described in Ref. [94]. The  $Z$ -VR and Top-VR requirements are summarized in Table 5.

The diboson background accounts for 26 % (43 %) of the total SM contribution in the SR-highMass (SR-lowMass) and mainly arises from  $WW \rightarrow \tau\nu\tau\nu$  and  $ZZ \rightarrow \tau\tau\nu\nu$  events, in which more than 96 % of the contribution is from events with two real tau leptons. To validate the MC modelling and normalisation of the  $WW$  ( $ZZ$ ) process, a validation region  $WW$ -VR ( $ZZ$ -VR) with enriched  $WW \rightarrow e\nu\mu\nu$  ( $ZZ \rightarrow ee\nu\nu$  or  $ZZ \rightarrow \mu\mu\nu\nu$ ) contribution is defined. For  $WW$ -VR, events with two isolated leptons ( $\ell = e$  or  $\mu$ ) with different flavor and opposite sign are selected, while for  $ZZ$ -VR, events with two isolated leptons with same flavor and opposite sign are selected. To keep a similar phase space as the SRs, the  $WW$ -VR ( $ZZ$ -VR) is defined to be close to the SRs except for the selected objects being a light lepton pair. Top-tagged events are vetoed to suppress  $t\bar{t}$  contribution in  $WW$ -VR. To suppress the  $Z$ +jets contribution in  $ZZ$ -VR,  $\Delta R(\ell, \ell) < 1.5$  is applied and  $|m_{\ell\ell} - m_Z| < 15 \text{ GeV}$  is used to enrich the  $ZZ$  contribution. The definitions of  $WW$ -VR and  $ZZ$ -VR are summarized in Table 6.

The purity of the selection in  $Z$ +jets and  $t\bar{t}$  events is above 80 % in the respective validation regions, and the purity of the selection in  $WW$  ( $ZZ$ ) events is around 65 % (92 %) in  $WW$ -VR ( $ZZ$ -VR). Good

agreement between the data and SM expectation is observed. The  $m_{T2}$  distribution in the Z-VR, Top-VR, WW-VR and ZZ-VR are shown in Figure 5.

Table 5: The Z-VR (left) and Top-VR (right) definitions.

Z-VR	Top-VR
at least one opposite sign tau lepton pair tau $p_T > 50, 40$ GeV $E_T^{\text{miss}} > 60$ GeV	
at least two medium tau leptons $b$ -jet veto $m_{T2} < 10$ GeV	at least one medium and one loose tau lepton at least 1 $b$ -jet $m_{T2} > 10$ GeV $m_{CT}$ top-tagged

Table 6: The WW-VR (left) and ZZ-VR (right) definitions.

WW-VR	ZZ-VR
one opposite sign lepton pair $\mu p_T > 30$ GeV, $e p_T > 40$ GeV jet veto $m_{\ell\ell} > 50$ GeV $E_T^{\text{miss}} > 50$ GeV $m_{T\mu} > 100$ GeV $m_{T2} > 70$ GeV	
two isolated leptons ( $e$ or $\mu$ ) with different flavor $m_{CT}$ top tag veto	two isolated leptons ( $e$ or $\mu$ ) with same flavor $\Delta R(\ell, \ell) < 1.5$ $ m_{\ell\ell} - m_Z  < 15$ GeV

## 7 Systematic uncertainties

Systematic uncertainties have an impact on the estimates of the background and signal event yields in the control and signal regions. Uncertainties arising from experimental effects, theoretical predictions, and modelling are evaluated.

The main sources of experimental uncertainties on the SM background estimates include tau lepton- and jet-energy calibrations and resolution, tau lepton identification, pile-up, and uncertainties related to the modelling of  $E_T^{\text{miss}}$  in the simulation. The uncertainties on the energy and momentum scale of each of the objects entering the  $E_T^{\text{miss}}$  calculation are evaluated, as well as the uncertainties on the soft term resolution and scale. The main contributions to experimental systematic uncertainties in the SR-lowMass (SR-highMass) are from the tau lepton identification and energy scale around 6 % (8 %), jet energy scale and resolution around 11 % (4 %),  $E_T^{\text{miss}}$  soft term resolution and scale around 2 % (6 %), and pile-up around 8 % (8 %). Other contributions are less than 3 %.

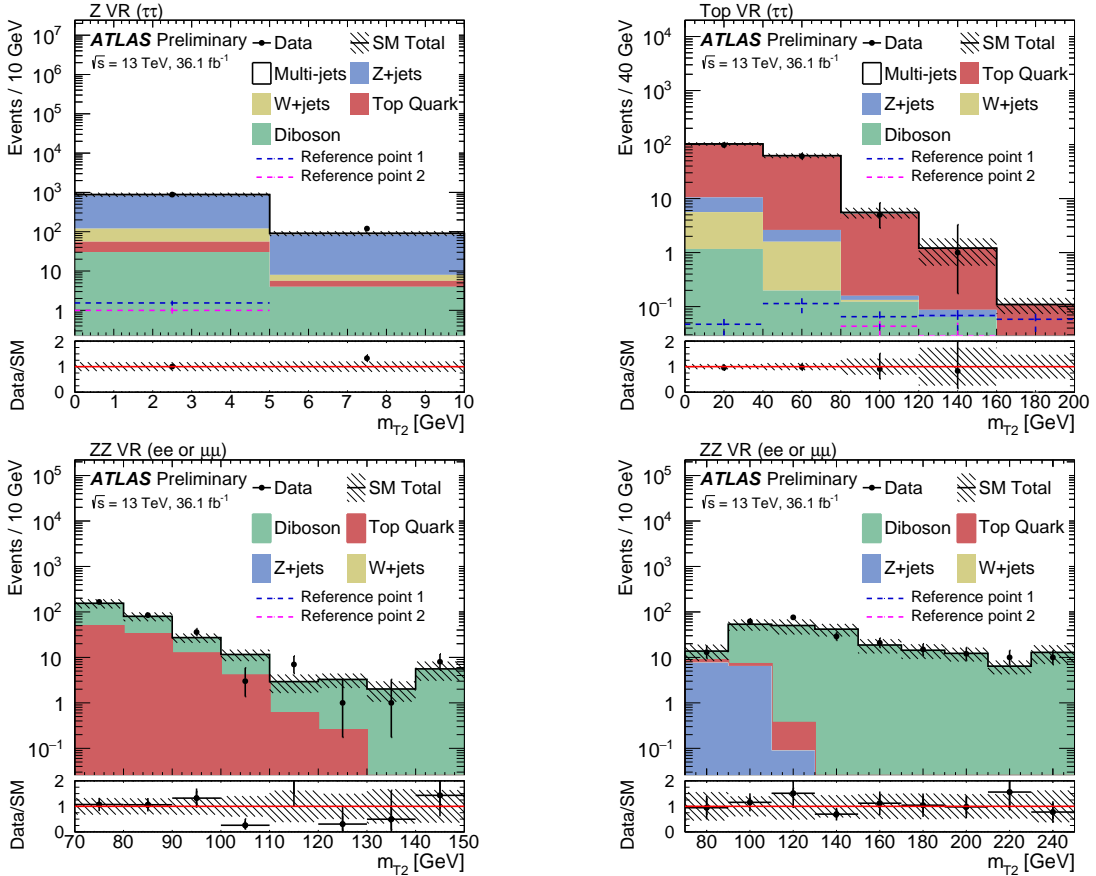


Figure 5: The  $m_{T2}$  distribution in the  $Z$ -VR (top left), Top-VR (top right),  $WW$ -VR (bottom left) and  $ZZ$ -VR (bottom right). The SM backgrounds other than multi-jet production are estimated from MC simulation and normalised to  $36.1 \text{ fb}^{-1}$ . The multi-jet contribution is negligible and not considered in  $WW$ -VR and  $ZZ$ -VR, while in  $Z$ -VR and Top-VR it is estimated from data using the ABCD method, using CRs obtained with the same technique used for the SRs, and described in Section 6.1. The hatched bands represent the combined statistical and systematic uncertainties on the total SM background. For illustration, the distributions of the SUSY reference points (defined in Section 3) are also shown as dashed lines. The lower panels show the ratio of data to the SM background estimate. The last bin includes the overflow.

Theoretical uncertainties affecting the Monte Carlo generator predictions are evaluated from variation of the renormalisation and factorisation scales, and the impact of the resummation scale and merging scale of the matrix element with the parton shower. For  $W$ +jets and diboson processes, the uncertainties related to the choice of QCD renormalisation and factorisation scales are determined from the comparison of the nominal samples with samples with these scales varied up and down by a factor of two. Uncertainties in the resummation scale and the matching scale between the matrix elements and parton shower are evaluated by varying up and down the corresponding parameters in **SHERPA** by a factor of two. For  $W$ +jets events, the uncertainty due to the jet- $p_T$  threshold used for parton–jet matching is calculated by comparing the baseline samples with jet  $p_T$  threshold set to 20 GeV to samples with a threshold of 15 or 30 GeV. **SHERPA** is compared with **MADGRAPH** to evaluate the uncertainty related to the generator choice for  $W$ +jets production. The total theoretical uncertainty for diboson processes in the SRs is around 15 %, mainly coming from the choice of the QCD renormalisation scale (4–9 %) and resummation scale (around 10 %). The theory uncertainty on  $W$ +jets production is 13–20 %, and the main source is the generator uncertainty (4–17 %) and the QCD renormalisation scale (9–10 %). An overall systematic uncertainty of 6 % in the inclusive cross section is assigned to the diboson process. Based on previous studies [29], a total theoretical uncertainty of 25 % is assigned for the top quarks and  $Z$ +jets contributions to the SRs.

Several sources of systematic uncertainty are considered for the ABCD method used to determine the multi-jet background: the correlation between the tau-id, the charge requirement, and the kinematic variables  $m_{T2}$ , the limited number of events in the CRs, and the subtraction of other SM backgrounds. The systematic uncertainty on the correlation is estimated by comparing the transfer factor from CR-B to CR-C to that of VR-E to VR-F. The systematic uncertainty on the non-multi-jet background subtraction in the control regions is estimated by considering the systematic uncertainty of the MC estimations of the non-multi-jet background in the CRs. Both uncertainties are of the order of 10 %. The systematic uncertainty in the signal region due to the limited number of events in the control regions is estimated by taking the statistical uncertainty of the event yields in these control regions. It corresponds to the largest source of uncertainty for the ABCD method, and it reaches 21–42 % for CR-A.

The dominant systematic uncertainties on the total background predictions in the signal regions are associated with the normalisation uncertainties on the multi-jet background (around 32 % in both SR-lowMass and SR-highMass), and the statistical uncertainty on MC predictions, which are 18 % in SR-lowMass and 24 % in SR-highMass respectively.

The total uncertainty in the signal yield for the SUSY reference points defined in Section 3 is around 20 %. The main source of experimental uncertainties are the tau lepton identification and energy scale, jet energy scale and resolution,  $E_T^{\text{miss}}$  soft term resolution and scale, and pile-up, they account for about 15 %. Only the cross section uncertainty is taken into account for signal processes and it varies from 3 % to 20 % for the considered SUSY models. SUSY models with higher chargino mass have larger uncertainties.

## 8 Statistical analysis

The statistical interpretation of the results is performed using the profile likelihood method implemented in the **HistFitter** framework [95]. Three types of fits are performed for each SR.

- The *background-only* fit uses as an input the number of observed events in the multi-jet CR-A and  $W$ -CR, the expected SM contributions to the multi-jet CR-A and  $W$ -CR, and the transfer factors, which relate the number of multi-jet or  $W$ +jets events in their associated control region to that

predicted in the signal region. The free parameters in the fit are the normalisations of the  $W$ +jets and multi-jet contributions. The signal is assumed to be absent in this fit.

- A *model-independent limit* fit combines the data event yield in the SR with the SM background estimate and its uncertainties obtained by the background-only fit to test the presence of any non-SM signal that contributes to the SR. The significance of a possible excess of observed events over the SM prediction is quantified by the one-sided probability,  $p(\text{signal} = 0)$  denoted as  $p_0$ , of the background alone to fluctuate to the observed number of events or higher using the asymptotic formula described in Ref. [91]. The presence of a non-SM signal will manifest itself in a small value for  $p_0$ .
- In the *model-dependent limit* fit the SUSY signal is allowed to populate both the signal and the control regions, and it is scaled by a freely floating signal normalisation factor. The background normalisation factors are also determined simultaneously in the fit. A SUSY model with a specific set of sparticle masses is rejected if the upper limit of the signal normalisation factor obtained in this fit is smaller than unity.

The likelihood function is a product of the probability density functions, one for each region contributing to the fit. The number of events in a given CR or SR is described using a Poisson distribution, the mean of which is the sum of the expected contributions from all background sources. The systematic uncertainties on the expected event yields are included as nuisance parameters and are assumed to be Gaussian distributed with a width determined from the size of the uncertainty. Correlations between control and signal regions, and background processes are taken into account with common nuisance parameters. The fit parameters are determined by maximising the product of the Poisson probability functions and the constraints for the nuisance parameters.

## 9 Results

The observed number of events in each signal region and the expected contributions from SM processes are given in Table 7. The contributions of multi-jet and  $W$ +jets events are scaled with the normalisation factors obtained from the background-only fit described in Section 8. The multi-jet normalisation in the SR-lowMass (SR-highMass) is compatible with 1 and has an uncertainty of around 100 % (86 %), due to the limited number of observed events in the multi-jet CR-A. The  $W$ +jets normalisation is  $1.02 \pm 0.15$ . The  $m_{T2}$  distribution is shown in Figure 6 for data, SM expectations, and the SUSY reference points defined in Section 3. In both signal regions, observations and background expectations are found to be compatible within uncertainties.

Carrying out the model-independent fit, upper limits at 95 % confidence level (CL) on the number of non-SM events in the SRs are derived. All limits are calculated using the  $\text{CL}_s$  prescription [96]. Normalising these by the integrated luminosity of the data sample, they can be interpreted as upper limits on the visible non-SM cross section,  $\sigma_{\text{vis}}^{95}$ , which is defined as the product of acceptance, reconstruction efficiency and production cross section. The accuracy of the limits obtained by the asymptotic formula was tested for all SRs by randomly generating a large number of pseudo-datasets and repeating the fit. Good agreement was found.

Table 7: Observed and expected number of events in the signal regions for  $36.1 \text{ fb}^{-1}$ . The contributions of multi-jet and  $W$ -jets events are scaled with the normalisation factors obtained from the background-only fit described in Section 8. Expected event yields for the SUSY reference points (defined in Section 3) are also given. The shown uncertainties are the sum in quadrature of statistical and systematic uncertainties. The correlation of systematic uncertainties among control regions and among background processes is fully taken into account. The one-sided  $p_0$ -values, the observed and expected 95 % CL upper limits on the visible non-SM cross section ( $\sigma_{\text{vis}}^{95}$ ), and the number of signal events ( $S_{\text{obs}}^{95}$ ) are given. Values of  $p_0 > 0.5$  are truncated to  $p_0 = 0.5$ .

SM process	SR-lowMass	SR-highMass
diboson	$5.9 \pm 2.2$	$1.0 \pm 0.8$
$W$ -jets	$1.8 \pm 1.1$	$0.7 \pm 0.5$
Top quark	$1.2 \pm 1.0$	$0.03^{+0.26}_{-0.03}$
$Z$ -jets	$0.6^{+0.7}_{-0.6}$	$0.6 \pm 0.5$
multi-jet	$4.3 \pm 4.0$	$1.3 \pm 1.1$
SM total	$14 \pm 6$	$3.7 \pm 1.4$
Observed	10	5
Reference point 1	$11.6 \pm 2.6$	$11.8 \pm 2.8$
Reference point 2	$10.0 \pm 2.1$	$11.4 \pm 2.6$
$p_0$	0.5	0.3
Expected $\sigma_{\text{vis}}^{95}$ [fb]	$0.31^{+0.12}_{-0.08}$	$0.17^{+0.08}_{-0.05}$
Observed $\sigma_{\text{vis}}^{95}$ [fb]	0.26	0.20

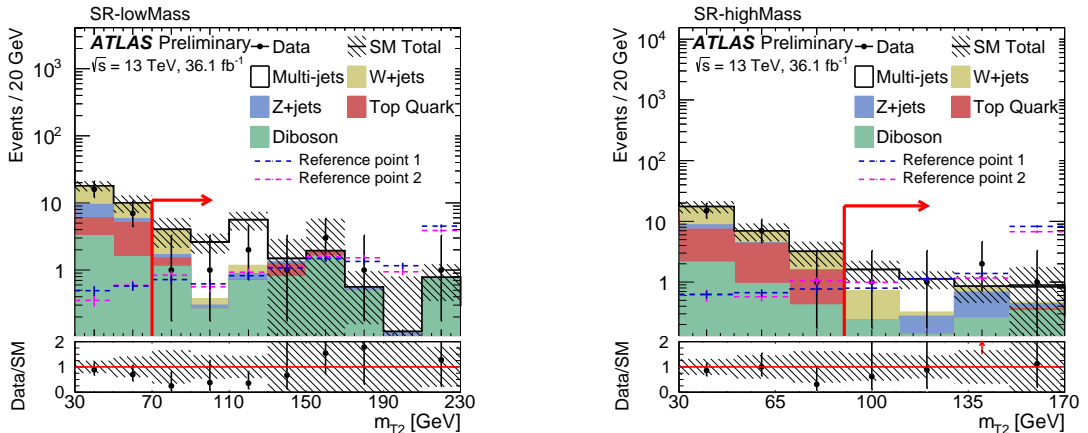


Figure 6: The  $m_{\text{T}2}$  distribution before the  $m_{\text{T}2}$  requirement is applied for SR-lowMass (left) and SR-highMass (right), where the arrow indicates the position of the cut in the signal region. The stacked histograms show the expected SM backgrounds normalised to  $36.1 \text{ fb}^{-1}$ . The multi-jet contribution is estimated from data using the ABCD method. The contributions of multi-jet and  $W$ -jets events are scaled with the corresponding normalisation factors. The hatched bands represent the sum in quadrature of systematic and statistical uncertainties on the total SM background. For illustration, the distributions of the SUSY reference points (defined in Section 3) are also shown as dashed lines. The lower panels show the ratio of data to the total SM background estimate. The last bin includes the overflow.

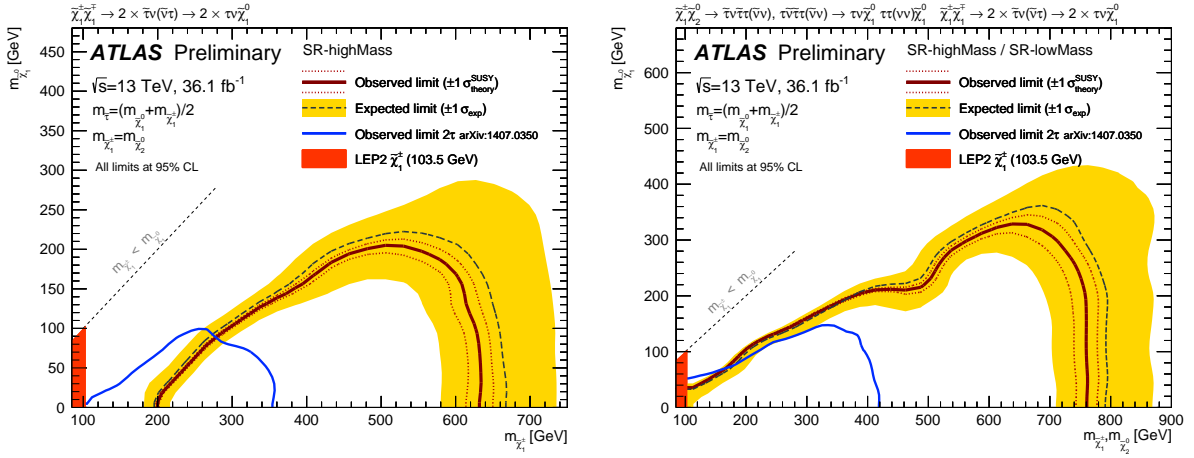


Figure 7: 95 % CL exclusion contours for simplified models with  $\tilde{\chi}_1^+ \tilde{\chi}_1^-$  production (left) and production of  $\tilde{\chi}_1^+ \tilde{\chi}_1^-$  and  $\tilde{\chi}_1^\pm \tilde{\chi}_2^0$  (right). See text for details of exclusion curves and uncertainty bands. The LEP limit on the chargino mass is also shown. Results are compared with the observed limits obtained by previous ATLAS searches [29] as blue contours.

## 10 Interpretation

In the absence of a significant excess over the SM background expectations, the observed and expected numbers of events in the signal regions are used to place exclusion limits at 95 % CL using the model-dependent limit fit described in Section 8. SR-highMass is used to derive limits for  $\tilde{\chi}_1^+ \tilde{\chi}_1^-$  production and SR-highMass and SR-lowMass are used to derive limits for the production of  $\tilde{\chi}_1^+ \tilde{\chi}_1^-$  and  $\tilde{\chi}_1^\pm \tilde{\chi}_2^0$ . The exclusion limits for the simplified models described in Section 3 are shown in Figure 7. Only  $\tilde{\chi}_1^+ \tilde{\chi}_1^-$  production is assumed for the left plot, whereas both production processes are considered simultaneously for the right plot. The solid (dashed) lines show the observed (expected) exclusion contours. The band around the expected limit shows the  $\pm 1\sigma$  variations, including all uncertainties except theoretical uncertainties on the signal cross section. The dotted lines around the observed limit indicate the sensitivity to  $\pm 1\sigma$  variations of the theoretical uncertainties on the signal cross section.

Chargino masses up to 630 GeV are excluded for a massless lightest neutralino in the scenario of direct production of chargino pairs. In the case of production of chargino pairs and mass-degenerate charginos and next-to-lightest neutralinos, chargino masses up to 760 GeV are excluded for a massless lightest neutralino. These limits significantly extend previous results [29, 30] in the high chargino mass region.

## 11 Conclusion

Searches for the electroweak production of supersymmetric particles in events with at least two hadronically decaying tau leptons are performed using  $36.1 \text{ fb}^{-1}$  of  $pp$  collision data at  $\sqrt{s} = 13 \text{ TeV}$  recorded with the ATLAS experiment at the Large Hadron Collider. Agreement between data and SM expectations is observed in all signal regions. These results are used to set limits on the visible cross section for events beyond the Standard Model in each signal region.

Exclusion limits are placed on parameters of the simplified models. Chargino masses up to 630 GeV are excluded for a massless lightest neutralino in the scenario of direct production of wino-like chargino pairs, with each chargino decaying into the lightest neutralino via an intermediate on-shell stau or tau sneutrino. In the case of production of chargino pairs and mass-degenerate charginos and next-to-lightest neutralinos, common  $\tilde{\chi}_1^\pm$ - $\tilde{\chi}_2^0$  masses up to 760 GeV are excluded for a massless lightest neutralino.

## References

- [1] Yu. A. Golfand and E. P. Likhtman, *Extension of the Algebra of Poincare Group Generators and Violation of  $p$  Invariance*, JETP Lett. **13** (1971) 323–326, [Pisma Zh. Eksp. Teor. Fiz. 13, 452 (1971)].
- [2] D. V. Volkov and V. P. Akulov, *Is the Neutrino a Goldstone Particle?*, Phys. Lett. B **46** (1973) 109–110.
- [3] J. Wess and B. Zumino, *Supergauge Transformations in Four-Dimensions*, Nucl. Phys. B **70** (1974) 39–50.
- [4] J. Wess and B. Zumino, *Supergauge Invariant Extension of Quantum Electrodynamics*, Nucl. Phys. B **78** (1974) 1.
- [5] S. Ferrara and B. Zumino, *Supergauge Invariant Yang-Mills Theories*, Nucl. Phys. B **79** (1974) 413.
- [6] A. Salam and J. A. Strathdee, *Supersymmetry and Nonabelian Gauges*, Phys. Lett. B **51** (1974) 353–355.
- [7] S. P. Martin, *A Supersymmetry primer*, arXiv:hep-ph/9709356 [hep-ph], [Adv. Ser. Direct. High Energy Phys. 18, 1 (1998)].
- [8] G. R. Farrar and P. Fayet, *Phenomenology of the Production, Decay, and Detection of New Hadronic States Associated with Supersymmetry*, Phys. Lett. B **76** (1978) 575–579.
- [9] G. Jungman, M. Kamionkowski, and K. Griest, *Supersymmetric Dark Matter*, Physics Reports **267** (1996) 195–373.
- [10] H. Goldberg, *Constraint on the Photino Mass from Cosmology*, Phys. Rev. Lett. **50** (1983) 1419, [Erratum: Phys. Rev. Lett. 103, 099905 (2009)].
- [11] J. R. Ellis, J. S. Hagelin, D. V. Nanopoulos, K. A. Olive, and M. Srednicki, *Supersymmetric Relics from the Big Bang*, Nucl. Phys. B **238** (1984) 453–476.
- [12] L. Evans and P. Bryant, *LHC Machine*, JINST **3** (2008) S08001.
- [13] D. Albornoz Vásquez, G. Bélanger, and C. Böhm, *Revisiting light neutralino scenarios in the MSSM*, Phys. Rev. D **84** (2011) 095015, arXiv:1108.1338 [hep-ph].
- [14] G. Belanger, F. Boudjema, A. Cottrant, A. Pukhov, and A. Semenov, *WMAP constraints on SUGRA models with non-universal gaugino masses and prospects for direct detection*, Nucl. Phys. B **706** (2005) 411, arXiv:hep-ph/0407218 [hep-ph].
- [15] S. King, J. Roberts, and D. Roy, *Natural dark matter in SUSY GUTs with non-universal gaugino masses*, JHEP **0710** (2007) 106, arXiv:0705.4219 [hep-ph].
- [16] M. Dine and W. Fischler, *A Phenomenological Model of Particle Physics Based on Supersymmetry*, Phys. Lett. B **110** (1982) 227.
- [17] L. Alvarez-Gaume, M. Claudson, and M. B. Wise, *Low-Energy Supersymmetry*, Nucl. Phys. B **207** (1982) 96.
- [18] C. R. Nappi and B. A. Ovrut, *Supersymmetric Extension of the  $SU(3) \times SU(2) \times U(1)$  Model*, Phys. Lett. B **113** (1982) 175.

[19] M. Dine and A. E. Nelson, *Dynamical supersymmetry breaking at low-energies*, *Phys. Rev. D* **48** (1993) 1277, [arXiv:hep-ph/9303230](https://arxiv.org/abs/hep-ph/9303230).

[20] M. Dine, A. E. Nelson, and Y. Shirman, *Low-energy dynamical supersymmetry breaking simplified*, *Phys. Rev. D* **51** (1995) 1362, [arXiv:hep-ph/9408384](https://arxiv.org/abs/hep-ph/9408384).

[21] M. Dine, A. E. Nelson, Y. Nir, and Y. Shirman, *New tools for low-energy dynamical supersymmetry breaking*, *Phys. Rev. D* **53** (1996) 2658, [arXiv:hep-ph/9507378](https://arxiv.org/abs/hep-ph/9507378).

[22] L. Randall and R. Sundrum, *Out of this world supersymmetry breaking*, *Nucl. Phys. B* **557** (1999) 79–118, [arXiv:hep-th/9810155](https://arxiv.org/abs/hep-th/9810155) [hep-th].

[23] G. F. Giudice, M. A. Luty, H. Murayama, and R. Rattazzi, *Gaugino mass without singlets*, *JHEP* **12** (1998) 027, [arXiv:hep-ph/9810442](https://arxiv.org/abs/hep-ph/9810442) [hep-ph].

[24] MSSM Working Group Collaboration, A. Djouadi et al., *The Minimal supersymmetric standard model: Group summary report*, in *GDR (Groupement De Recherche) - Supersymetrie Montpellier, France, April 15-17, 1998*. 1998. [arXiv:hep-ph/9901246](https://arxiv.org/abs/hep-ph/9901246) [hep-ph].  
[https://inspirehep.net/record/481987/files/arXiv:hep-ph\\_9901246.pdf](https://inspirehep.net/record/481987/files/arXiv:hep-ph_9901246.pdf).

[25] C. F. Berger, J. S. Gainer, J. L. Hewett, and T. G. Rizzo, *Supersymmetry without prejudice*, *JHEP* **02** (2009) 023, [arXiv:0812.0980](https://arxiv.org/abs/0812.0980) [hep-ph].

[26] J. Alwall, M.-P. Le, M. Lisanti, and J. G. Wacker, *Searching for directly decaying gluinos at the Tevatron*, *Phys. Lett. B* **666** (2008) 34–37, [arXiv:0803.0019](https://arxiv.org/abs/0803.0019) [hep-ph].

[27] J. Alwall, P. Schuster, and N. Toro, *Simplified models for a first characterization of new physics at the LHC*, *Phys. Rev. D* **79** (2009) 075020, [arXiv:0810.3921](https://arxiv.org/abs/0810.3921) [hep-ph].

[28] LHC New Physics Working Group Collaboration, D. Alves, *Simplified models for LHC New physics searches*, *J. Phys. G* **39** (2012) 105005, [arXiv:1105.2838](https://arxiv.org/abs/1105.2838) [hep-ph].

[29] ATLAS Collaboration, *Search for the direct production of charginos, neutralinos and staus in final states with at least two hadronically decaying taus and missing transverse momentum in pp collisions at  $\sqrt{s} = 8$  TeV with the ATLAS detector*, *JHEP* **10** (2014) 096, [arXiv:1407.0350](https://arxiv.org/abs/1407.0350) [hep-ex].

[30] CMS Collaboration, *Searches for electroweak production of charginos, neutralinos, and sleptons decaying to leptons and W, Z, and Higgs bosons in pp collisions at 8 TeV*, *Eur. Phys. J. C* **74** (2014) 3036, [arXiv:1405.7570](https://arxiv.org/abs/1405.7570) [hep-ex].

[31] CMS Collaboration, *Search for supersymmetry in events with soft leptons, low jet multiplicity, and missing transverse energy in proton–proton collisions at  $\sqrt{s} = 8$  TeV*, *Phys. Lett. B* **759** (2016) 9, [arXiv:1512.08002](https://arxiv.org/abs/1512.08002) [hep-ex].

[32] The LEP SUSY Working Group and the ALEPH, DELPHI, L3 and OPAL experiments notes LEPSUSYWG/01-03.1, 04-01.1, <http://lepsusy.web.cern.ch/lepsusy/Welcome.html>.

[33] ALEPH Collaboration, S. Schael, et al., *Absolute mass lower limit for the lightest neutralino of the MSSM from  $e^+e^-$  data at  $\sqrt{s}$  up to 209 GeV*, *Phys. Lett. B* **583** (2004) 247–263.

[34] DELPHI Collaboration, J. Abdallah, et al., *Searches for supersymmetric particles in  $e^+e^-$  collisions up to 208 GeV and interpretation of the results within the MSSM*, *Eur. Phys. J. C* **31** (2003) 421–479.

[35] L3 Collaboration, M. Acciarri, et al., *Search for charginos and neutralinos in  $e^+e^-$  collisions at  $\sqrt{s} = 189$  GeV*, *Phys. Lett. B* **472** (2000) 420–433.

[36] OPAL Collaboration, G. Abbiendi, et al., *Search for chargino and neutralino production at  $\sqrt{s} = 192$  GeV to 209 GeV at LEP*, *Eur. Phys. J. C* **35** (2004) 1–20.

[37] ATLAS Collaboration, *The ATLAS Experiment at the CERN Large Hadron Collider*, *JINST* **3** (2008) S08003.

[38] ATLAS Collaboration, *ATLAS Insertable B-Layer Technical Design Report*, CERN-LHCC-2010-013. ATLAS-TDR-19, 2010, <http://cds.cern.ch/record/1291633>.

[39] ATLAS Collaboration, *2015 start-up trigger menu and initial performance assessment of the ATLAS trigger using Run-2 data*, ATL-DAQ-PUB-2016-001, 2016, <https://cds.cern.ch/record/2136007/>.

[40] ATLAS Collaboration, *Luminosity determination in  $pp$  collisions at  $\sqrt{s} = 8$  TeV using the ATLAS detector at the LHC*, *Eur. Phys. J. C* **76** (2016) 653, <arXiv:1608.03953> [hep-ex].

[41] Gleisberg, T. et al., *Event generation with SHERPA 1.1*, *JHEP* **02** (2009) 007, <arXiv:0811.4622> [hep-ph].

[42] S. Höche, F. Krauss, M. Schonherr, and F. Siegert, *QCD matrix elements + parton showers: The NLO case*, *JHEP* **04** (2013) 027, <arXiv:1207.5030> [hep-ph].

[43] T. Gleisberg and S. Höche, *Comix, a new matrix element generator*, *JHEP* **12** (2008) 039, <arXiv:0808.3674> [hep-ph].

[44] F. Caccioli, P. Maierhofer, and S. Pozzorini, *Scattering Amplitudes with Open Loops*, *Phys. Rev. Lett.* **108** (2012) 111601, <arXiv:1111.5206> [hep-ph].

[45] S. Schumann and F. Krauss, *A Parton shower algorithm based on Catani-Seymour dipole factorisation*, *JHEP* **03** (2008) 038, <arXiv:0709.1027> [hep-ph].

[46] Ball, Richard D. et al., *Parton distributions for the LHC Run II*, *JHEP* **04** (2015) 040, <arXiv:1410.8849> [hep-ph].

[47] ATLAS collaboration, *Single Boson and Diboson Production Cross Sections in  $pp$  Collisions at  $\sqrt{s} = 7$  TeV*, ATL-COM-PHYS-2010-695, 2010, <https://cds.cern.ch/record/1287902/>.

[48] H.-L. Lai et al., *New parton distributions for collider physics*, *Phys. Rev. D* **82** (2010) 074024, <arXiv:1007.2241> [hep-ph].

[49] ATLAS Collaboration, *Multi-boson simulation for 13 TeV ATLAS analyses*, ATL-PHYS-PUB-2016-002, 2016, <https://cds.cern.ch/record/2119986>.

[50] S. Alioli, P. Nason, C. Oleari, and E. Re, *A general framework for implementing NLO calculations in shower Monte Carlo programs: the POWHEG BOX*, *JHEP* **06** (2010) 043, <arXiv:1002.2581> [hep-ph].

[51] T. Sjostrand, S. Mrenna, and P. Z. Skands, *PYTHIA 6.4 physics and manual*, *JHEP* **05** (2006) 026, <arXiv:hep-ph/0603175> [hep-ph].

[52] P. Z. Skands, *Tuning Monte Carlo Generators: The perugia tunes*, *Phys. Rev. D* **82** (2010) 074018, <arXiv:1005.3457> [hep-ph].

[53] D. J. Lange, *The EvtGen particle decay simulation package*, *Nucl. Instrum. Meth.* **A462** (2001) 152.

[54] M. Czakon and A. Mitov, *Top++: A program for the calculation of the top-pair cross-section at hadron colliders*, *Comput. Phys. Commun.* **185** (2014) 2930, [arXiv:1112.5675 \[hep-ph\]](https://arxiv.org/abs/1112.5675).

[55] N. Kidonakis, *Two-loop soft anomalous dimensions for single top quark associated production with a W- or H-*, *Phys. Rev.* **D82** (2010) 054018, [arXiv:1005.4451 \[hep-ph\]](https://arxiv.org/abs/1005.4451).

[56] Kant, P. et al., *HatHor for single top-quark production: Updated predictions and uncertainty estimates for single top-quark production in hadronic collisions*, *Comput. Phys. Commun.* **191** (2015) 74–89, [arXiv:1406.4403 \[hep-ph\]](https://arxiv.org/abs/1406.4403).

[57] Alwall, J. et al., *The automated computation of tree-level and next-to-leading order differential cross sections, and their matching to parton shower simulations*, *JHEP* **07** (2014) 079, [arXiv:1405.0301 \[hep-ph\]](https://arxiv.org/abs/1405.0301).

[58] T. Sjostrand, S. Mrenna, and P. Z. Skands, *A brief introduction to PYTHIA 8.1*, *Comput. Phys. Commun.* **178** (2008) 852–867, [arXiv:0710.3820 \[hep-ph\]](https://arxiv.org/abs/0710.3820).

[59] ATLAS Collaboration, *ATLAS Pythia 8 tunes to 7 TeV data*, ATL-PHYS-PUB-2014-021, 2014, <https://cds.cern.ch/record/1966419>.

[60] R. D. Ball et al., *Parton distributions with LHC data*, *Nucl. Phys.* **B867** (2013) 244–289, [arXiv:1207.1303 \[hep-ph\]](https://arxiv.org/abs/1207.1303).

[61] A. Lazopoulos, T. McElmurry, K. Melnikov, and F. Petriello, *Next-to-leading order QCD corrections to  $t\bar{t}Z$  production at the LHC*, *Phys. Lett.* **B666** (2008) 62–65, [arXiv:0804.2220 \[hep-ph\]](https://arxiv.org/abs/0804.2220).

[62] J. M. Campbell and R. K. Ellis,  *$t\bar{t}W^{+-}$  production and decay at NLO*, *JHEP* **07** (2012) 052, [arXiv:1204.5678 \[hep-ph\]](https://arxiv.org/abs/1204.5678).

[63] L. Lönnblad and S. Prestel, *Matching tree-level matrix elements with interleaved showers*, *JHEP* **03** (2012) 019, [arXiv:1109.4829 \[hep-ph\]](https://arxiv.org/abs/1109.4829).

[64] B. Fuks, M. Klasen, D. R. Lamprea, and M. Rothering, *Gaugino production in proton-proton collisions at a center-of-mass energy of 8 TeV*, *JHEP* **1210** (2012) 081, [arXiv:1207.2159 \[hep-ph\]](https://arxiv.org/abs/1207.2159).

[65] B. Fuks, M. Klasen, D. R. Lamprea, and M. Rothering, *Precision predictions for electroweak superpartner production at hadron colliders with Resummino*, *Eur.Phys.J.* **C73** (2013) 2480, [arXiv:1304.0790 \[hep-ph\]](https://arxiv.org/abs/1304.0790).

[66] Borschensky, Christoph et al., *Squark and gluino production cross sections in pp collisions at  $\sqrt{s} = 13, 14, 33$  and 100 TeV*, *Eur. Phys. J. C* **74** (2014) 3174, [arXiv:1407.5066 \[hep-ph\]](https://arxiv.org/abs/1407.5066).

[67] ATLAS Collaboration, *The ATLAS Simulation Infrastructure*, *Eur. Phys. J. C* **70** (2010) 823, [arXiv:1005.4568 \[hep-ex\]](https://arxiv.org/abs/1005.4568).

[68] S. Agostinelli et al., *GEANT4: A simulation toolkit*, *Nucl. Instrum. Meth.* **A506** (2003) 250–303.

[69] ATLAS Collaboration, *The simulation principle and performance of the ATLAS fast calorimeter simulation FastCaloSim*, ATL-PHYS-PUB-2010-013, 2010, <https://cds.cern.ch/record/1300517>.

[70] ATLAS Collaboration, *Summary of ATLAS Pythia 8 tunes*, ATL-PHYS-PUB-2012-003, 2012, <https://cds.cern.ch/record/1474107>.

[71] A. D. Martin, W. J. Stirling, R. S. Thorne, G. Wat, *Parton distributions for the LHC*, Eur. Phys. J. **C63** (2009) 189, [arXiv:0901.0002 \[hep-ph\]](https://arxiv.org/abs/0901.0002).

[72] ATLAS Collaboration, *Vertex Reconstruction Performance of the ATLAS Detector at  $\sqrt{s} = 13$  TeV*, ATL-PHYS-PUB-2015-026, 2015, <https://cds.cern.ch/record/2037717>.

[73] ATLAS Collaboration, *Topological cell clustering in the ATLAS calorimeters and its performance in LHC Run 1*, [arXiv:1603.02934 \[hep-ex\]](https://arxiv.org/abs/1603.02934).

[74] M. Cacciari, G. P. Salam, and G. Soyez, *The anti- $k_T$  jet clustering algorithm*, JHEP **0804** (2008) 063, [arXiv:0802.1189 \[hep-ph\]](https://arxiv.org/abs/0802.1189).

[75] M. Cacciari and G. P. Salam, *Dispelling the  $N^3$  myth for the  $k_t$  jet-finder*, Phys. Lett. **B 641** (2006) 57, [arXiv:hep-ph/0512210 \[hep-ph\]](https://arxiv.org/abs/hep-ph/0512210).

[76] ATLAS Collaboration, *Jet energy measurement with the ATLAS detector in proton–proton collisions at  $\sqrt{s} = 7$  TeV*, Eur. Phys. J. **C 73** (2013) 2304, [arXiv:1112.6426 \[hep-ex\]](https://arxiv.org/abs/1112.6426).

[77] ATLAS Collaboration, *Jet Calibration and Systematic Uncertainties for Jets Reconstructed in the ATLAS Detector at  $\sqrt{s} = 13$  TeV*, ATL-PHYS-PUB-2015-015, 2015, <https://cds.cern.ch/record/2037613>.

[78] M. Cacciari and G. P. Salam, *Pileup subtraction using jet areas*, Phys. Lett. **B 659** (2008) 119, [arXiv:0707.1378](https://arxiv.org/abs/0707.1378).

[79] ATLAS Collaboration, *Tagging and suppression of pileup jets with the ATLAS detector*, ATLAS-CONF-2014-018, 2014, <https://cds.cern.ch/record/1700870>.

[80] ATLAS Collaboration, *Performance of b-jet identification in the ATLAS experiment*, JINST **11** (2016) P04008, [arXiv:1512.01094 \[hep-ex\]](https://arxiv.org/abs/1512.01094).

[81] ATLAS Collaboration, *Expected performance of the ATLAS b-tagging algorithms in Run-2*, ATL-PHYS-PUB-2015-022, 2015, <https://cds.cern.ch/record/2037697>.

[82] ATLAS Collaboration, *Optimisation of the ATLAS b-tagging performance for the 2016 LHC Run.*, ATL-PHYS-PUB-2016-012, 2016, <https://cds.cern.ch/record/2160731>.

[83] ATLAS Collaboration, *Electron efficiency measurements with the ATLAS detector using the 2015 LHC proton–proton collision data*, ATLAS-CONF-2016-024, 2016, <https://cds.cern.ch/record/2157687>.

[84] ATLAS Collaboration, *Muon reconstruction performance of the ATLAS detector in proton–proton collision data at  $\sqrt{s} = 13$  TeV*, Eur. Phys. J. **C 76** (2016) 292, [arXiv:1603.05598 \[hep-ex\]](https://arxiv.org/abs/1603.05598).

[85] ATLAS Collaboration, *Reconstruction, Energy Calibration, and Identification of Hadronically Decaying Tau Leptons in the ATLAS Experiment for Run-2 of the LHC*, Tech. Rep. ATL-PHYS-PUB-2015-045, CERN, Geneva, Nov, 2015. <https://cds.cern.ch/record/2064383>.

[86] ATLAS Collaboration, *Identification and energy calibration of hadronically decaying tau leptons with the ATLAS experiment in pp collisions at  $\sqrt{s} = 8$  TeV*, Eur. Phys. J. **C 75** (2015) 303, [arXiv:1412.7086 \[hep-ex\]](https://arxiv.org/abs/1412.7086).

[87] ATLAS Collaboration, *Expected performance of missing transverse momentum reconstruction for the ATLAS detector at  $\sqrt{s} = 13$  TeV*, ATL-PHYS-PUB-2015-023, 2015, <https://cds.cern.ch/record/2037700>.

[88] ATLAS Collaboration, *Performance of missing transverse momentum reconstruction with the ATLAS detector in the first proton–proton collisions at  $\sqrt{s} = 13$  TeV*, ATL-PHYS-PUB-2015-027, 2015, <https://cds.cern.ch/record/2037904>.

[89] C. G. Lester and D. J. Summers, *Measuring masses of semi-invisibly decaying particles pair produced at hadron colliders*, *Phys. Lett.* **B463** (1999) 99–103, [arXiv:hep-ph/9906349](https://arxiv.org/abs/hep-ph/9906349).

[90] A. Barr, C. Lester, and P. Stephens, *A variable for measuring masses at hadron colliders when missing energy is expected;  $m_{T2}$ : the truth behind the glamour*, *J. Phys.* **G29** (2003) 2343–2363, [arXiv:hep-ph/0304226](https://arxiv.org/abs/hep-ph/0304226).

[91] G. Cowan, K. Cranmer, E. Gross, and O. Vitells, *Asymptotic formulae for likelihood-based tests of new physics*, *Eur. Phys. J.* **C71** (2011) 1554, [arXiv:1007.1727 \[physics.data-an\]](https://arxiv.org/abs/1007.1727).

[92] ATLAS Collaboration, *Muon reconstruction performance in early  $\sqrt{s} = 13$  TeV data*, ATL-PHYS-PUB-2015-037, 2015, <https://cds.cern.ch/record/2047831>.

[93] D. Tovey, *On measuring the masses of pair-produced semi-invisibly decaying particles at hadron colliders*, *JHEP* **0804** (2008) 034.

[94] G. Polesello and D. Tovey, *Supersymmetric particle mass measurement with the boost-corrected contransverse mass*, *JHEP* **1003** (2010) 030.

[95] M. Baak, G. Besjes, D. Côte, A. Koutsman, J. Lorenz, et al., *HistFitter software framework for statistical data analysis*, *Eur. Phys. J.* **C75** (2015) 153, [arXiv:1410.1280 \[hep-ex\]](https://arxiv.org/abs/1410.1280).

[96] A. L. Read, *Presentation of search results: the CLs technique*, *J. Phys.* **G 28** (2002) 2693.